Journal of Innovative Optical Health Sciences
Vol. 9, No. 3 (2016) 1641001 (8 pages)

DOI: 10.1142/S1793545816410017

World Scientific
www.worldscientific.com

Effect of light polariztion on pattern illumination super-resolution imaging

Caimin Qiu, Jianling Chen, Zexian Hou, Chaoxian Xu,
Shusen Xie and Hongqin Yang*
Key Laboratory of Optoelectronic Science
and Technology for Medicine of Ministry of Education
Provincial Key Laboratory for Photonics Technology
Institute of Laser and Optoelectronics Technology
Fujian Normal University, Fuzhou 350007, P. R. China
**hqyang@fjnu.edu.cn*

Received 25 August 2015
Accepted 2 December 2015
Published 28 March 2016

Far-field fluorescence microscopy has made great progress in the spatial resolution, limited by light diffraction, since the super-resolution imaging technology appeared. And stimulated emission depletion (STED) microscopy and structured illumination microscopy (SIM) can be grouped into one class of the super-resolution imaging technology, which use pattern illumination strategy to circumvent the diffraction limit. We simulated the images of the beads of SIM imaging, the intensity distribution of STED excitation light and depletion light in order to observe effects of the polarized light on imaging quality. Compared to fixed linear polarization, circularly polarized light is more suitable for SIM on reconstructed image. And right-handed circular polarization (CP) light is more appropriate for both the excitation and depletion light in STED system. Therefore the right-handed CP light would be the best candidate when the SIM and STED are combined into one microscope. Good understanding of the polarization will provide a reference for the patterned illumination experiment to achieve better resolution and better image quality.

Keywords: Structured illumination microscopy; stimulated emission depletion microscopy; polarized light; diffraction limit.

1. Introduction

Fluorescence microscopy is widely used in life-science field. However, the spatial resolution of conventional fluorescence microscopy is limited because of the diffraction of light, which is called the Abbe diffraction limit.[1] Over the past decade the researchers have developed several super resolution techniques, such as stimulated emission depletion (STED)

*Corresponding author.

microscopy,[2,3] structured illumination microscopy (SIM),[4,5] photoactivated localization microscopy (PALM).[6] and stochastic optical reconstruction microscopy (STORM)[7] to circumvent the diffraction limit. And these super resolution techniques can be divided into two categories. The STED and SIM techniques are based on patterned illumination. In this category of techniques, a patterned light is applied to the sample to modulate its fluorescence emission. And the PALM and STORM use single-molecule imaging and locating method to obtain the center of the single molecule to achieve super resolution imaging. So the accuracy of the locating method is related to the resolution, and the brightness of the used dye can also affect accuracy of the locating method. Therefore locating algorithm and fluorescent dye are the key factors to affect the resolution of this kind of super resolution technique. However, the wavelength, frequency, polarization, amplitude and phase of the illumination beam have effects on the patterned light. Here, we focus on the effect of light polarization on patterned illumination super resolution techniques.

The polarization of light in structured illumination was employed to enable single-shot optical sectioning by utilizing polarization-maintaining properties of fluorescent dyes, which was called polarized illumination coded structured illumination (pico-SIM).[8] And three-beam interference with circular polarization (CP) for SIM was proposed to provide isotropic illumination and routinely maintained modulation contrast at all orientations without a complicated polarization rotator.[9]

In STED microscopy, circular polarized beam was widely used in generation of either 2D or 3D super-resolution spots.[10] However, cylindrical vector beams, especially radially polarized beam and azimuthally polarized beam, gained more attention in STED microscopy recently.[11–13] The researchers also studied the relationship between the polarization of the beam and the size of the dark focal spot.[14]

Some researchers have applied the STED to the nonlinear SIM.[15,16] And the two techniques may be combined within one microscope for different purposes of super resolution imaging. This manuscript aims to analyze the optimal beam polarization when the two super resolution techniques are combined within one microscope through computer simulation. To demonstrate the influence of polarized light of different modes on the quality of images of SIM and STED, we simulated images of fluorescence beads for SIM and scanning spot of the excitation light and depletion light with polarization for STED.

2. Two Pattern Illumination Super-Resolution Imaging Modes

2.1. *SIM*

The principle and image reconstruction algorithm of SIM were briefly given based on that of Gustafsson.[4] The detection fluorescence distribution $D(r)$ is a convolution of the distribution of fluorescent emission $E(r)$ with the point spread function $H(r)$ of the system,

$$D(r) = (E \otimes H)(r) \tag{1}$$

And if an object is excited with illumination intensity $I(r)$, and the density distribution of fluorescent dye is $S(r)$, the resulting emission fluorescence distribution is

$$E(r) = S(r)I(r) \tag{2}$$

and the illumination intensity distribution of two-beam interference is described as[9]

$$\begin{aligned} &I[r(x,y,z),\theta,\beta] \\ &= 2I_1 + \frac{1}{2}\left[\begin{array}{l}\left(\dfrac{2}{1+e^2}\right)(\cos^2\beta + \cos 2\theta \sin^2\beta) \\ +\left(\dfrac{2e^2}{1+e^2}\right)(\cos^2\beta - \cos 2\theta \sin^2\beta)\end{array}\right] \\ &\quad \times 2I_1 \cos\begin{pmatrix} 2kx\cos\theta\sin\beta \\ +2ky\sin\theta\sin\beta + 2\varphi \end{pmatrix}, \end{aligned} \tag{3}$$

where $k = 2\pi/\lambda$, ellipticity $e = x/y$; x and y correspond to the lengths of the semi-major and semi-minor axes; $e = 0$ and 1 represent linear polarization (LP) and CP, respectively. Here, the expressions of the intensity distribution of the left-handed CP and right-handed CP are the same. φ is the initial phase of the illumination light. Half of the angle between the two first-order beams is interaction angle β, which is set at 40°. θ is the pattern orientation.

Accordingly, the corresponding spectrum in frequency space is described by

$$D(k) = (S(k) \otimes I(k))OTF(k), \tag{4}$$

where $D(k)$, $S(k)$, $I(k)$ and $OTF(k)$ are Fourier transforms of $D(r)$, $S(r)$, $I(r)$ and $H(r)$.

The expression $I(r)$ in Eq. (3) represents the intensity distribution of two-beam interference. And its Fourier transform $I(k)$ contains 0 and ± 1 order high frequency information. So the observable emission spectrum of the formula (4) contains three spectrum components of sample structure: the zero-order component with the same information as the conventional image; ± 1 order high frequency components with encoded super-resolution information. By changing the illumination phase and capturing three images at different phases, we can separate the three high frequency components. And then the ± 1 order high frequency components are shifted to the right position, then the three components are superimposed to obtain the extended spectrum. However, the spectrum is extended only in one illumination direction. By repeating the above procedure for other illumination orientations, the extended spectrum of the other direction is obtained to restore the isotropic resolution improvement. And the inverse Fourier transform is applied to the extended spectrum to obtain the super resolution image. And for detailed information please see Ref. 4.

2.2. *STED Microscopy*

The complex amplitude of the Gaussian beam at the input plane can be written as

$$E_0(\gamma,\theta) = A_0 \exp\left(-\gamma^2 \frac{\sin^2\theta}{\sin^2\alpha}\right), \tag{5}$$

where, A_0 is the amplitude of the Gaussian beam, $\gamma = a/w$ is the truncation parameter, that denotes the fraction of the beam inside the aperture, with a as the aperture radius and ω as the beam size at waist. θ is the conic angle (the angle between the optical axis and the given ray), α is the maximum semi-aperture angle of the objective, and the numerical aperture $NA = n\sin\theta_{\max}$, n is the refractive index. Using the vectorial Debye theory, the field distribution of the point near focus is given by[17]

$$\begin{aligned} E(x,y,z) = -\frac{iC}{\lambda}\int_0^{\alpha}\int_0^{2\pi} & E_0\sqrt{\cos\theta}A_1(\theta,\varphi) \\ & \times \exp[ikn(x\sin\theta\cos\varphi + y\sin\theta\sin\varphi + z\cos\theta)] \\ & \times \phi_s(\theta,\varphi)P(\theta,\varphi)\sin\theta d\theta d\varphi. \end{aligned} \tag{6}$$

Here, C is related to the optical system parameters, λ is the wavelength in the medium, And $k = 2\pi/\lambda$ is the wave number. $(x,\ y,\ z)$ are the Cartesian coordinates of the point in the focal region. $A_1(\theta,\ \varphi)$ represents the wavefront aberration function, here we ignore the aberration. So $A_1(\theta,\ \varphi) = 1$. $\phi_s(\theta,\ \varphi)$ is the phase delay of the phase mask inserted on STED beam. For a commonly used 0–2π vortex phase plate, the phase delay $\phi_s(\theta,\ \varphi) = \exp(i\varphi), 0 \le \varphi \le 2\pi$. And $P(\theta,\ \varphi)$ represents the polarization distribution of input light and can be expressed as

$$P(\theta,\varphi) = \begin{bmatrix} 1+(\cos\theta-1)\cos^2\varphi & (\cos\theta-1)\cos\varphi\sin\varphi \\ (\cos\theta-1)\cos\varphi\sin\varphi & 1+(\cos\theta-1)\sin^2\varphi \\ -\sin\theta\cos\varphi & -\sin\theta\sin\varphi \end{bmatrix} \begin{bmatrix} p_x \\ p_y \end{bmatrix}. \tag{7}$$

The Jones matrix of $\begin{bmatrix} p_x \\ p_y \end{bmatrix}$ of LP and CP can be expressed as[18]

X/Y LP:

$$\begin{bmatrix} p_x \\ p_y \end{bmatrix} = \begin{bmatrix} 1 \\ 0 \end{bmatrix} \quad \text{and} \begin{bmatrix} 0 \\ 1 \end{bmatrix}. \tag{8}$$

Right-hand/Left-hand CP:

$$\begin{bmatrix} p_x \\ p_y \end{bmatrix} = \frac{1}{\sqrt{2}}\begin{bmatrix} 1 \\ i \end{bmatrix} \quad \text{and} \quad \frac{1}{\sqrt{2}}\begin{bmatrix} 1 \\ -i \end{bmatrix}. \tag{9}$$

And, the intensity distribution of the point near focus could be calculated by

$$I = |\,E(x,y,z)\,|^2. \tag{10}$$

3. Results and Discussion

To demonstrate the effects of light polarization on SIM imaging, we simulated two-beam interference structured illumination with different polarization. In the simulation, the emission light wavelength is set at 520 nm, and the numerical-aperture is set at 0.8. Here, LP represents fixed LP without rotating polarization with pattern orientation. The beams of s-LP occurs only at pattern orientation $\theta = 0°$. The simulated sample is several randomly distributed 100 nm beads.

First, we simulated single pattern orientation with LP and CP. We found that the fixed LP of two first-order beams in pattern orientation 90° has the lowest modulation contrast. And the modulation contrast of CP in pattern orientation 90° is better than that of LP, as shown in Figs. 1(a) and 1(b). To quantitatively compare the resolution improvement of the different polarizations, we plotted the intensity profiles of the single bead along 90°

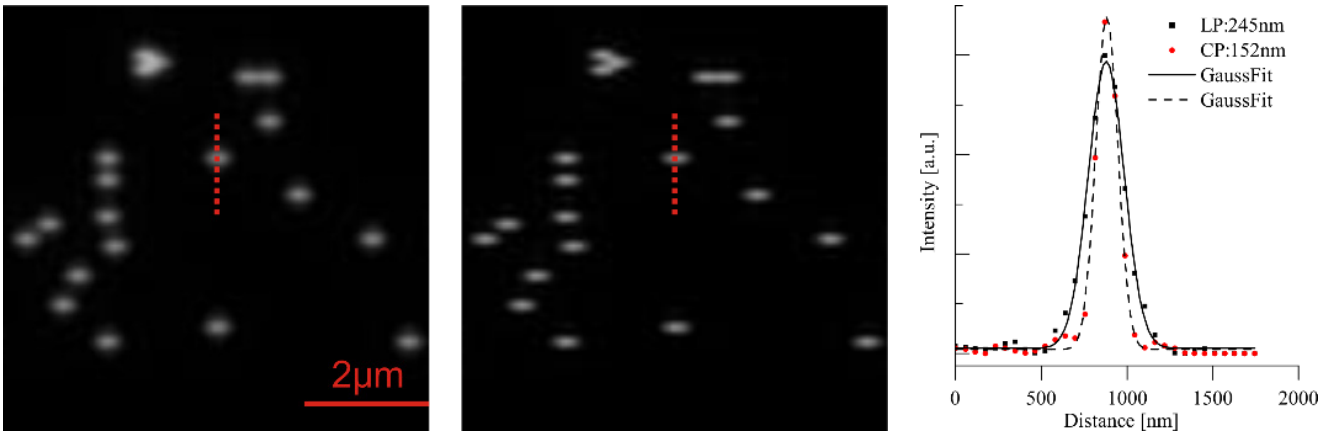

(a) (b) (c)

Fig. 1. Simulations of resolution improvement by structured illumination in pattern orientation 90°. (a) is the reconstructed result for fixed LP, (b) is for CP. (c) is the intensity profiles of single bead (red dotted line) in Figs. (a) and (b) along pattern orientation with Gaussian fit.

direction (red dotted line) with Gaussian fit, shown in Fig. 1(c). The FWHM of reconstructed LP and CP SI image are 245 nm and 152 nm, respectively. This result reflects that CP and LP have different modulation depths. And the modulation depth obviously affects the resolution improvement.

And we simulated three pattern orientations ($0° + 60° + 120°$) for isotropic resolution enhancement. The results of images of 100 nm fluorescence beads for conventional wide-field and SIM reconstructed from three pattern orientations of LP and CP are shown in Fig. 2. The conventional image and intensity distribution of the single bead (red arrow) are shown in Figs. 2(a) and 2(d). And Figs. 2(b) and 2(e), 2(c) and 2(f) show those reconstructed from LP and CP, respectively. As shown in Fig. 2(d), the FWHM of conventional image is ~ 320 nm. As shown in Figs. 2(e) and 2(f), the resolution improvement is nearly a factor of two, and the FWHM along 0° direction are 146 nm and 165 nm with LP and CP. However, the FWHM along 90° direction of CP is better than that of LP, which are 180 nm and 215 nm, respectively. And the FWHM of other directions are also calculated, for instance, 174 nm and 187 nm for LP and CP along 45° direction, and 172 nm and 166 nm for LP and CP along 135° direction. This result shows that the reconstructed images of CP have better isotropy than that of LP.

To explain the different reconstructed results with LP and CP, we find that the coefficient of $2I_1$ of the second term in Eq. (3) is difference between LP and CP. And the coefficient of $2I_1$ is called modulation contrast. We calculate the modulation contrast of interference with two beams in pattern orientation from 0° to 180° for LP and CP, which is shown in Fig. 3. As shown that the contrast has the maximum value 1 with orientation 0° and the minimum value about 0.174 with orientation 90° for LP. It is the different contrast that causes the FWHM of reconstructed image of LP with 0° orientation better than that with 90° orientation. And therefore the reconstructed image produces poor isotropy. However, the contrast has stable value about 0.59 for CP, which produces better isotropy.

To demonstrate the effects of light polarization on STED, we consider three kinds of typical polarized light, X-direction LP, right-handed and left-handed CP. And the simulated intensity distribution of excitation light with three kinds of typical polarized light is shown in Fig. 4. As shown in Fig. 4(d), the intensity distribution of linear polarized light is slightly elongated in the X-direction deviation. However, in Figs. 4(e) and 4(f), the intensity distribution of right-handed circular and left-handed circular polarized light is more uniform.

Figure 5 demonstrates the intensity distribution of depletion light with 0–2π vortex phase plate with three polarizations. As shown in Figs. 5(a) and 5(d), with LP the spot is not round, the intensity distribution is slightly elongated in the X direction deviation and the boundary is fuzzy. However, in Figs. 5(b) and 5(e), with right-handed CP the spot is round with a dark center and sharp boundary.

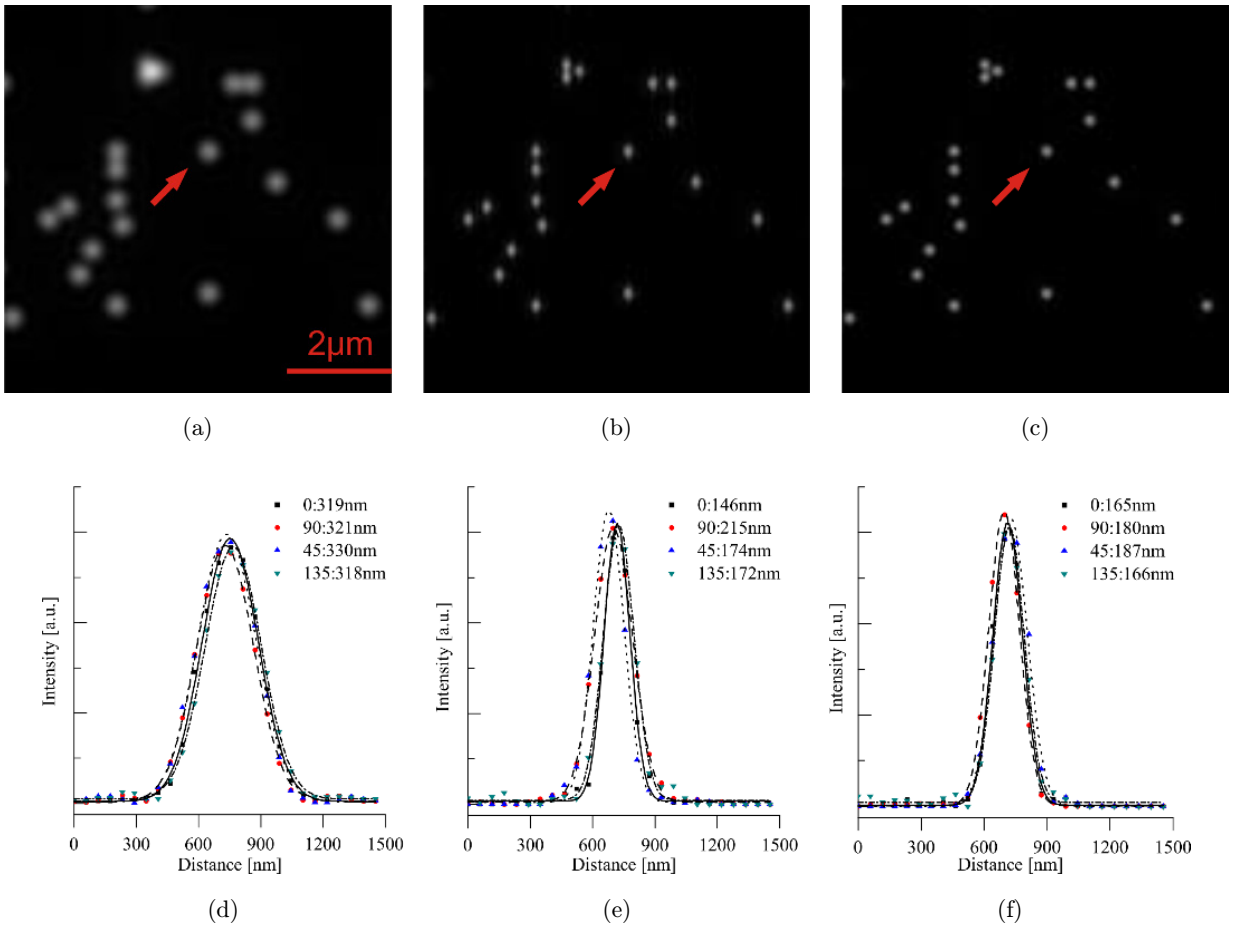

Fig. 2. Simulations of effects of polarization on reconstructed image. (a) and (d) are the image and intensity profiles of the bead (red arrow) with Gaussian fit for conventional wide-field microscopy. (b) and (c) are the SIM reconstructed images with three pattern orientations — 0°, 60° and 120° for fixed LP and CP. (e) and (f) are the intensity profiles of the bead (red arrow) with Gaussian fit for fixed LP and CP in (b) and (c). The intensity profiles are along 0°, 45°, 90°, 135° direction, respectively.

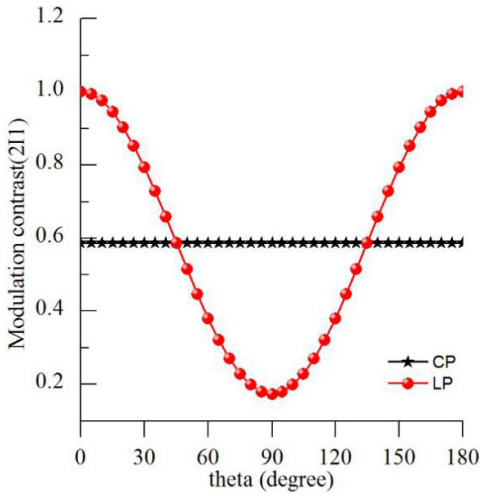

Fig. 3. Modulation contrast for interference with two beams for two case — CP and fixed LP in pattern orientation from 0° to 180°. The interaction angle β is 40°.

But in Figs. 5(c) and 5(f), the spot boundary is also round and sharp, but the center cannot reach darkness completely.

An ideal intensity distribution of STED beam is hoped to be a null intensity surrounded with a steep intensity profile at the periphery. The above results show that LP is not suitable for STED imaging, as it produces asymmetrical intensity distribution. Although the left-handed CP can create doughnut pattern, the center of the focal spot cannot achieve darkness completely, which would cause low efficiency of STED. And the right-handed CP can generate a zero intensity at center and a steep intensity profile at the periphery. Therefore, the right-handed CP is more appropriate for the STED microscopy. In summary, the right-handed CP would be the best candidate when the SIM and STED are combined into one microscope.

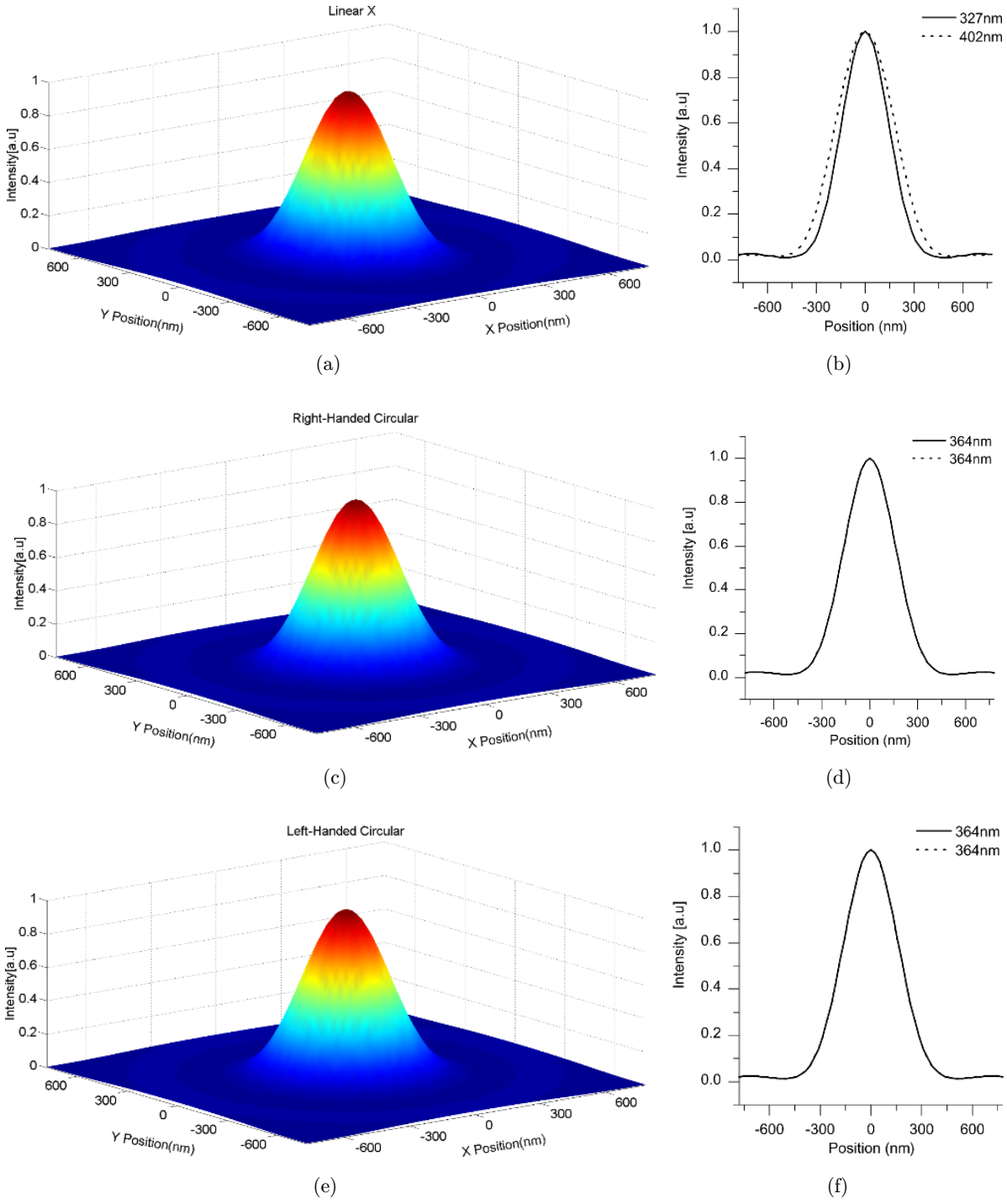

Fig. 4. Images of the scanning spot and normalized intensity distribution of excitation light with their different polarization on focus. (a), (b) and (c) correspond to LP (X-direction), right-handed CP and left-handed CP, respectively. The intensity distributions in (d), (e) and (f) are along the spot center $X = 0\,\text{nm}$ (solid line), $Y = 0\,\text{nm}$ (dot line) in (a), (b) and (c) respectively.

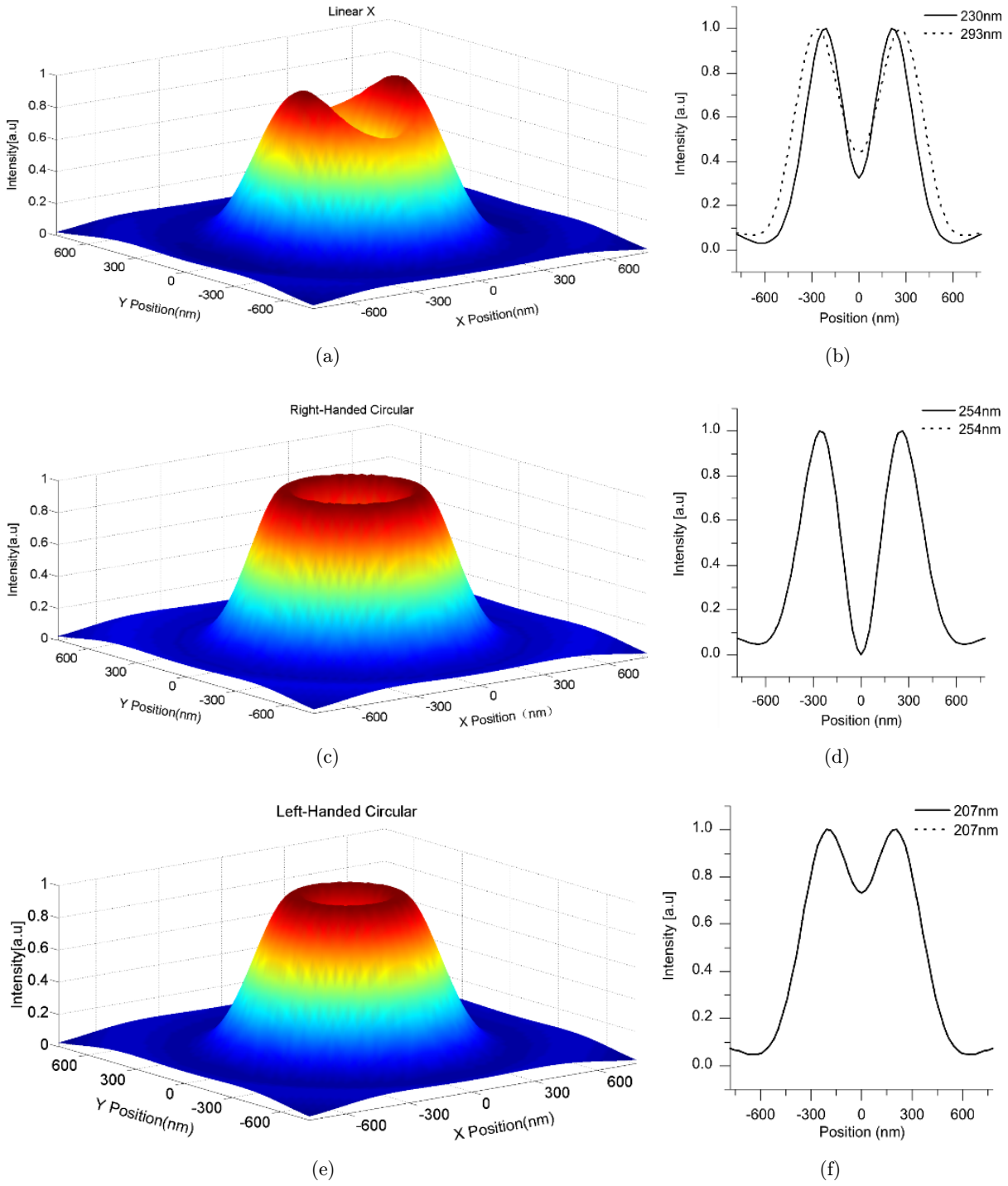

Fig. 5. Images of the scanning spot and normalized intensity distribution of different polarization on focus with a 0–2π vortex phase plate. (a), (b) and (c) correspond to the LP (X-direction), right-handed CP and left-handed CP, respectively. The intensity distributions in (d), (e) and (f) are along the spot center $X = 0$ nm (solid line), $Y = 0$ nm (dot line) in (a), (b) and (c) respectively.

4. Conclusions

In summary, we confirm that the polarization of illumination light has an effect on the patterned illumination super-resolution imaging. In SIM, we show that circularly polarized light is more suitable, compared to fixed LP, for SIM on reconstructed image quality, as the reconstructed image of CP has better isotropy than that of LP. And in STED, right-handed CP light is more appropriate for both the excitation and depletion light in STED system.

So, when the SIM and STED are combined with each other into one microscope, the right-handed CP light would be the best candidate. Through simulation, we are able to obtain the optimized polarization to guide experiments and achieve better resolution and better image quality.

Acknowledgments

This work was partly supported by the National Key Basic Research Program of China (973 project) under Grant No. 2015CB352006 and the National Natural Science Foundation of China under Grant Nos. 61335011 and 61405035 and Program for Changjiang Scholars and Innovative Research Team in University under Grant No. IRT_15R10.

References

1. E. Abbe, "Beiträge zur Theorie des Mikroskops und der mikroskopischen Wahrnehmung," *Archiv für mikro. Ana.* **9**, 413–418 (1873).
2. S. W. Hell, J. Wichmann, "Breaking the diffraction resolution limit by stimulated emission: Stimulated-emission–depletion fluorescence microscopy," *Opt. Lett.* **19**, 780–782 (1994).
3. T. A. Klar, S. W. Hell, "Subdiffraction resolution in far-field fluorescence microscopy," *Opt. Lett.* **24**, 954–956 (1999).
4. M. G. L. Gustafsson, D. A. Agard, J. W. Sedat, "Doubling the lateral resolution of wide-field fluorescence microscopy using structured illumination," *Proc. SPIE* **3919**, 141–150 (2000).
5. M. G. L. Gustafsson, "Surpassing the lateral resolution limit by a factor of two using structured illumination microscopy," *J. Microsc. Oxford* **198**, 82–87 (2000).
6. E. Betzig, G. H. Patterson, R. Sougrat, O. W. Lindwasser, S. Olenych, J. S. Bonifacino, M. W. Davidson, J. Lippincott-Schwartz, H. F. Hess, "Imaging intracellular fluorescent proteins at nanometer resolution," *Science* **313**, 1642–1645 (2006).
7. M. J. Rust, M. Bates, X. Zhuang, "Sub-diffraction-limit imaging by stochastic optical reconstruction microscopy (STORM)," *Nat. Methods* **3**, 793–796 (2006).
8. K. Wicker, R. Heintzmann, "Single-shot optical sectioning using polarization-coded structured illumination," *J. Optics UK* **12**, 084010 (2010).
9. H. Huang, B. Chang, L. Chou, S. Chiang, "Three-beam interference with circular polarization for structured illumination microscopy," *Opt. Express* **21**, 23963–23977 (2013).
10. B. Harke, C. K. Ullal, J. Keller, S. W. Hell, "Three-dimensional nanoscopy of colloidal crystals," *Nano Lett.* **8**, 1309–1313 (2008).
11. X. A. C. K. Yi, "A method for generating a three-dimensional dark spot using a radially polarized beam," *J. Optics-UK* **13**, 125704 (2011).
12. T. J. Gould, J. R. Myers, J. Bewersdorf, "Total internal reflection STED microscopy," *Opt. Express* **19**, 13351–13357 (2011).
13. M. Leutenegger, C. Ringemann, T. Lasser, S. W. Hell, C. Eggeling, "Fluorescence correlation spectroscopy with a total internal reflection fluorescence STED microscope (TIRF-STED-FCS)," *Opt. Express* **20**, 5243–5263 (2012).
14. X. Hao, C. Kuang, T. Wang, X. Liu, "Effects of polarization on the de-excitation dark focal spot in STED microscopy," *J. Optics UK* **12**, 115707 (2010).
15. H. Zhang, M. Zhao, L. Peng, "Nonlinear structured illumination microscopy by surface plasmon enhanced stimulated emission depletion," *Opt. Express* **19**, 24783–24794 (2011).
16. F. Dake, S. Nakayama, Y. Taki, "Theoretical assessment of two-dimensional nonlinear structured illumination microscopy based on structured excitation and structured stimulated emission depletion," *Opt. Rev.* **22**, 598–604 (2015).
17. B. Richards, E. Wolf, "Electromagnetic diffraction in optical systems. II. Structure of the image field in an aplanatic system," *Proceedings of the Royal Society of London A: Mathematical, Physical and Engineering Sciences* **253**, 358–379 (1959).
18. B. R. Boruah, M. Neil, "Focal field computation of an arbitrarily polarized beam using fast Fourier transforms," *Opt. Commun.* **282**, 4660–4667 (2009).